Journal of Power Sources 206 (2012) 204–209

Contents lists available at SciVerse ScienceDirect

Journal of Power Sources

journal homepage: www.elsevier.com/locate/jpowsour

Thermo-mechanical properties of (Sr,Y)TiO_3 as anode material for solid oxide fuel cells

B.X. Huang, V. Vasechko, Q.L. Ma, J. Malzbender*

Institute of Energy and Climate Research (IEK) Forschungszentrum Jülich GmbH, 52425 Jülich, Germany

ARTICLE INFO

Article history:
Received 4 October 2011
Received in revised form 19 January 2012
Accepted 24 January 2012
Available online 2 February 2012

Keywords:
Solid oxide fuel cells
Re-oxidation
Mechanical properties
Young's modulus
Strength
Fracture toughness

ABSTRACT

Low chemical expansion on re-oxidation makes (Sr,Y)TiO_3 a potential material for the application as anode for solid oxide fuel cells. Especially for the long term application mechanical stability is an important aspect. Micro-structural and mechanical testing results are presented for the material in the as-sintered reduced state and the state after subsequent oxidation. Crystalline structure and lattice constant was characterised by X-ray diffraction yielding the strain that will be induced by oxidation. Room temperature indentation testing permitted a determination of fracture toughness and Young's modulus, whereas the temperature dependence of the Young's modulus was measured with a resonance method up to 960 °C. The strength of the material was measured using ring-on-ring bending test. The fracture toughness as a function of temperature was measured using a combination of pre-indentation induced cracks and ring-on-ring bending test. Furthermore, the elastic modulus and critical strain were determined for porous material. Fracture surface and failure mode were characterised with supplementary scanning electron microscopy.

1. Introduction

Solid oxide fuel cells (SOFCs) can convert chemical energy directly into electricity with high efficiency and low environmental pollution. Hence, SOFCs have received considerable attentions in the last decades [1]. The actual design of a cell depends on the electrochemical performance of the materials, the available processing methods and for the mechanically supporting component, also on mechanical strength and reliability.

The widely used anode-supported planar design has great advantages for practical application since it offers a high electrical power output at a comparatively low operating temperature [2]. In the anode supported design a thick (300 μm–1.5 mm) porous anode substrate supports the thin anode functional layer (usually with lower porosity), the electrolyte and the cathode layer. A substrate porosity of ~30% is required to permit sufficient gas supply to the electrochemically active sites of the functional anode layer.

A main disadvantage of the frequently used Ni-YSZ anodes is the rather large re-oxidation strain. The re-oxidation induced strain for anode supported Ni-YSZ cells typically leads to electrolyte failure. In fact, it has been suggested that the strain should be < 0.1% to avoid electrolyte cracking [3]. The chemical expansion of the new anode material $Sr_{0.895}Y_{0.07}TiO_3$ (SYT) has reported to be only 0.14% at 800 °C when changing from wet Ar/4% H_2 to air [4], making this material in terms of re-oxidation stability an interesting alternative to Ni-YSZ.

For the analysis and simulation of the mechanical behavior, elastic modulus and fracture strength are critical parameters and in terms of a more basic fracture mechanics approach, the fracture toughness, which quantifies the resistance of a material against fracture and is independent of sample size [5]. As a guideline the properties of Ni-YSZ anode substrates might be used, where characteristic strengths (fracture stress for a failure probability of 63.2%) between ~100 and 500 MPa have been reported [6,7].

Since the strength is proportional to the fracture toughness the material behavior at elevated temperatures can be assessed using the room temperature fracture strength in combination with the temperature dependence of the fracture toughness. The current work reports the Young's modulus, fracture toughness and critical strain of SYT. In addition supporting micro-structural, X-ray diffraction (XRD), differential thermal analysis (DTA) and thermogravimetry (TG) results are reported.

2. Experiments

$Sr_{0.895}Y_{0.07}TiO_{3-\delta}$ (SYT) powder was prepared in amount of 1 kg per batch. Titanium (IV) isopropoxide (97%), $Sr(NO_3)_2$ (99.9%), $Y(NO_3)_3{\cdot}6\ H_2O$ (99.9%) were used as starting materials. The titanium (IV) isopropoxide was dropped into distilled water while it was stirred. The precipitate was filtered and washed, and then

* Corresponding author. Tel.: +49 2461616964; fax: +49 2461613699.
E-mail address: j.malzbender@fz-juelich.de (J. Malzbender).

0378-7753/$ – see front matter © 2012 Elsevier B.V. All rights reserved.
doi:10.1016/j.jpowsour.2012.01.137

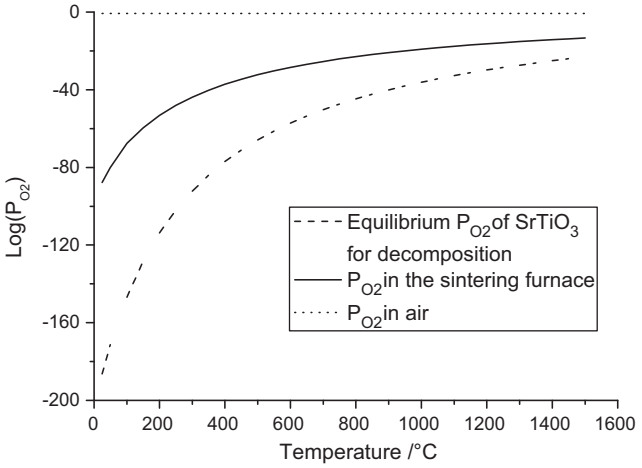

Fig. 1. Equilibrium P_{O2} for decomposition for $SrTiO_3$.

dissolved into HNO_3 solution. The Ti^{4+} concentration in this solution was determined by thermal gravimetry. Corresponding amounts of the nitrates were then added to the solution. After homogenization the solution was spray-pyrolysed in a commercial spray dryer (Nubilosa, Konstanz, Germany). After spray-pyrolysis the raw powder was heated up to 900 °C in air for 5 h.

The powder was then uniaxially pressed into rectangular bars (40 mm × 5 mm × 3 mm) or disks (⌀ ~22 mm, thickness 1 mm) and sintered in Ar/4% H_2 at 1400 °C for 5 h. The relative density of the bars was about 90%. Some of the powder was also coat-mixed and warm pressed [8] into plates with dimensions of 70 mm × 70 mm × 2 mm. After de-bindering and pre-sintering at 1250 °C in air, the plates were vacuum slip-cast with a YSZ electrolyte layer on the topside, then sintered in Ar/4% H_2 at 1400 °C for 5 h. The size of the plates after sintering was 50 mm × 50 mm × 1.5 mm with a YSZ layer thickness of 10–15 μm. These sintered half cells were then cut into smaller size of ~22 mm × 22 mm. For the sintering process in Ar/4% H_2, the oxygen partial pressure (P_{O2}) was calculated with Factsage. The resulting P_{O2} in the furnace is shown in Fig. 1 ($P_{O2} = P_{O2}/P^0$, P^0 is the standard pressure 1 atm).

Depth-sensitive indentation testing was used to determine hardness, Young's modulus on the basis of the relationships given in [9]. The methodology for hardness and Young's modulus measurements from depth-sensitive indentation tests is based on ISO 14577. Experiments were carried out using both a Fischer HC100 indentation system and a combined nano-micro indentation set-up (CSM, Switzerland). In addition depth-sensitive indentation testing was also used to determine fracture toughness values based on a direct measurement of the crack length after impression [9–11] using the relationship after [10,11] also given in [9] and the so-called indentation strength method (ISM), where the fracture stress of a pre-indented specimen is used to determine the fracture toughness [12,13] based on the procedure in [14], which permits to assess the temperature dependence of the fracture toughness [14]. The approach combines a defined pre-cracking of a sample with the subsequent measurement of the fracture stress in a bending test. In the absence of residual indentation induced stresses the fracture toughness can then be derived straight forward from the measured fracture stress [13].

The ring-on-ring testing is used for fracture stress measurements of disk-shaped brittle materials [15,16]. Biaxial ring-on-ring bending test followed the procedure given in ISO 1288 permitting a simultaneous assessment of elastic modulus. All tests were carried out with fixed support and load ring diameters (D_s = 15 mm, D_l = 7 mm). The calculation of Young's modulus E and fracture strength was based on the relevant standard (see ISO 1288).

Young's modulus of bar samples was determined using an impulse excitation method. The measurements were carried out with a Grindosonic equipment (Lemmens KG, Belgium) based on ASTM E 1876-01.

The electrical conductivity of the bars was measured by the DC four-probe method in the temperature range of 25–350 °C in Ar/4% H_2 with 3% H_2O. The crystal structure and lattice constant was characterized by XRD diffraction. Differential thermal analysis (DTA) and thermogravimetry (TG) (STA 449C Jupiter Netzsch) were carried out in air with heating rates of 2 K min^{-1}.

3. Results and discussion

In the following sections the results related to the stability, mechanical properties and conductivity of dense SYT are discussed, emphasising also the effect of the oxidation state of the material. The final section concentrates on the effect of the porosity on Young's modulus, strength and critical strain.

3.1. Stability

A first stage to the analysis of the material behaviour is an assessment of its chemical stability. The equilibrium O_2 partial pressure ($P_{O2} = P_{O2}/P^0$, P^0 is the standard pressure 1 atm) for the dissociation of $SrTiO_3$ calculated with the software Factsage is shown in Fig. 1. The oxygen partial pressure to be expected in the furnace is higher than the equilibrium P_{O2} for dissociation from RT to sintering temperature. Therefore, $SrTiO_3$ is not expected to dissociate and should remain in the oxidized state under this atmosphere. Since the composition of SYT is very close to $SrTiO_3$, it can be concluded that SYT should not decompose, which is also verified for the as-produced (reduced) state by TG measurement.

DTA/TG was carried out for as-received dense samples in air from RT to 1000 °C, and the heating/cooling rate was 2 K min^{-1}. The material was in the reduced state at the starting of the test. The weight increases obviously in the temperature range 600 °C to 950 °C during heating in the first thermal cycle, but keeps stable in the following cycles (Fig. 2a). Since the sample was sintered in reducing atmosphere, the weight increase is attributed to the oxidation of the sample. The change of weight is not observed in the second and third cycles, which suggests that the material does not release oxygen anymore in air up to 1000 °C. Assuming that only oxygen is released and absorbed with changing P_{O2}, and that the composition in air is $Y_{0.07}Sr_{0.895}TiO_3$, the initial composition in the reduced state is calculated on the basis of the weight change to be $Y_{0.07}Sr_{0.895}TiO_{2.97}$. Hence, the change of oxygen stoichiometry δ is only 0.03 from reduced atmosphere to air. The DTA curve continuously decreases from RT to 1000 °C. Although a slope change is observed at ~870 °C in DTA curve (Fig. 2b), no indication of a phase transition is found.

A SEM investigation revealed that there is a perovskite matrix phase with second phase inclusions (Fig. 3a). The average grain size of the perovskite material is 3 ± 1 μm. Energy dispersive X-ray diffraction (Table 1) revealed that the composition of perovskite matrix phase is in agreement with the composition proposed above $Y_{0.067}Sr_{0.9315}TiO_3$ and the second phase is TiO_2, which could not be indicated as additional diffraction peaks in a XRD analysis due to its low amount.

Room temperature XRD measurements of the lattice constant of as-received (reduced) SYT and oxidized SYT showed that both exhibit a cubic symmetry, with lattice constants of 0.3902 nm and 0.3910 nm, respectively, which yields a chemical strain on oxidation of ~0.2%.

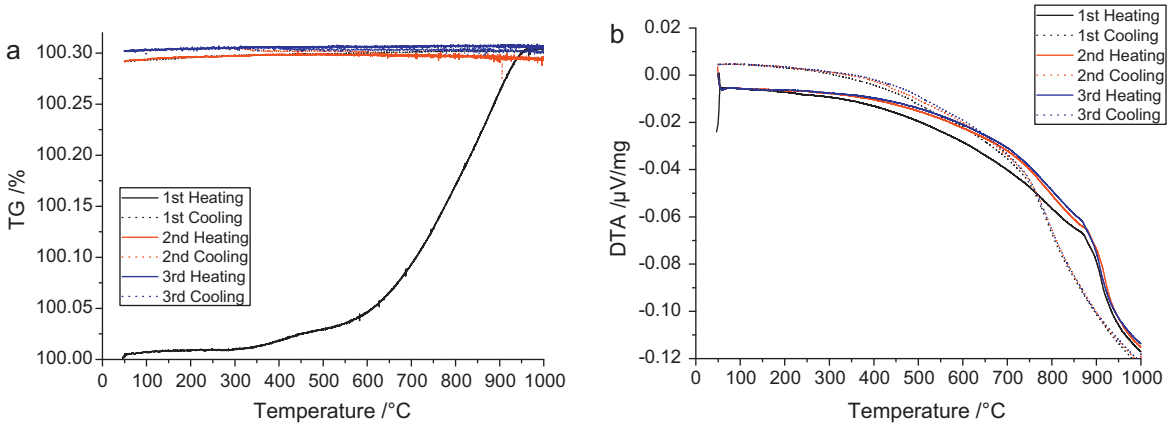

Fig. 2. (a) TG and (b) DTA curve of $Y_{0.07}Sr_{0.895}TiO_3$, heated in air.

3.2. Mechanical properties

Indentation testing was used to measure Young's modulus and hardness of as-received samples. Young's modulus and hardness appeared to be rather independent of load with average values of ~170 ± 10 GPa and 7 ± 1 GPa, respectively. The hardness increases below 300 mN due to indentation size effects. For loads above 0.3 N shear slip planes were observed within the grains surrounding the impressions (Fig. 3b). These slip planes were encountered for grains sizes larger than ~8 μm. Their orientation should be in agreement with the slip systems for the perovskite crystal lattice.

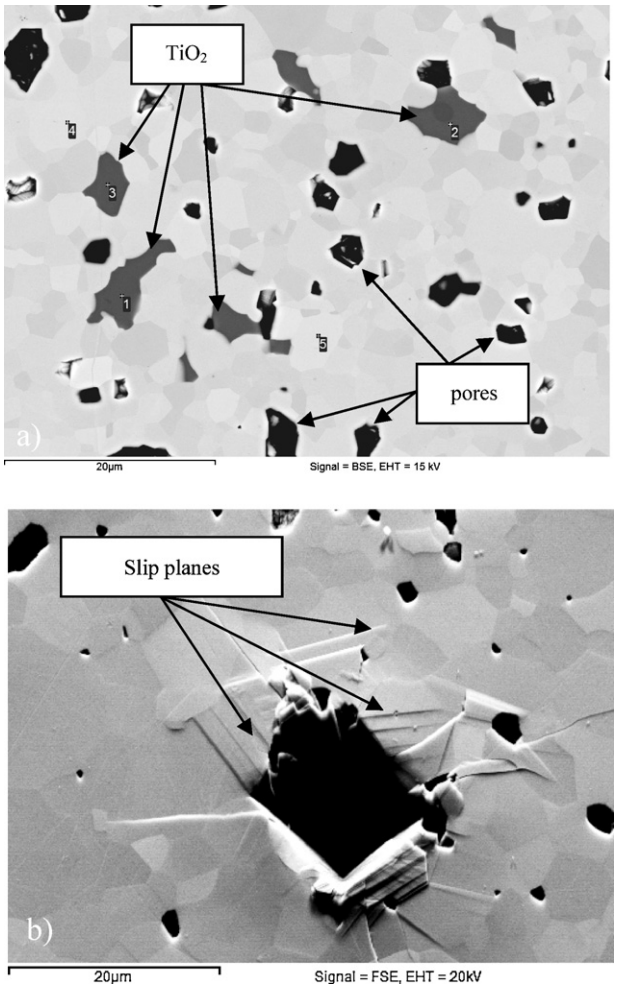

Fig. 3. (a) SEM based micro-structural image of $Y_{0.07}Sr_{0.895}TiO_3$ (EDX data in Table 1) and (b) slip planes in $Y_{0.07}Sr_{0.895}TiO_3$ grains after microindentation.

In addition the macroscopic the Young's modulus was determined on the basis of a resonance based method. The Young's modulus measurement of the reduced material in air from RT to 960 °C (Fig. 4a) yielded identical result for the heating and cooling process, which implies that the sample remains in the reduced state up to 960 °C due to the low diffusion rate of oxygen in the dense material. The value of the Young's modulus at RT is consistent with indentation test result. The Young's modulus increases by ~20% from RT to 220 °C, with a corresponding peak in the internal friction (Fig. 5b). It decreases slightly from 300 °C to 960 °C similar to polycrystalline ceramics without grain boundary softening, where a decrease of ~1% per hundred has been reported [17].

To investigate the Young's modulus of oxidized material, a specimen was pre-annealed in air at 1300 °C for 6 h. The Young's modulus of this oxidized sample increases from RT to 70 °C, and then exhibits similar slight decrease with increasing temperature similar as in the case of the reduced sample (Fig. 4a). A peak of internal friction is also observed along with the slight Young's modulus increase up to 70 °C (Fig. 4b). If the curve of oxidized sample would be shifted horizontally by 150 K, Young's modulus and internal friction of both samples would agree very well (Fig. 4). This might suggest that the same transition takes place for both samples, and only the transition temperature is shifted in dependence of the oxygen stoichiometry.

In addition to the resonance frequency based measurement, the temperature dependence of the Young's modulus was also determined from ring-on-ring bending test data (Fig. 5). The data are basically consistent with the values measured with resonance method.

The indentation fracture toughness of as-received samples as measured from the length of cracks after the impression as outlined in [9] was also independent of load (0.3 to 1 N) within the limits of uncertainty with an average value of ~0.7 ± 0.1 MPa $m^{0.5}$. In addition, ring-on-ring fracture tests with pre-indented specimens were

Table 1
Data obtained using EDX for the positions marked in Fig. 4a, all results in atomic %.

Spectrum	O	Al	Ti	Sr	Y
1	64.3	0.6	32.0	3.1	0.0
2	64.5	0.7	31.9	2.9	0.0
3	64.8	0.6	31.7	3.0	0.0
4	60.1	0.0	20.0	18.8	1.2
5	60.3	0.0	19.9	18.5	1.4
6	60.0	0.0	20.0	18.6	1.4

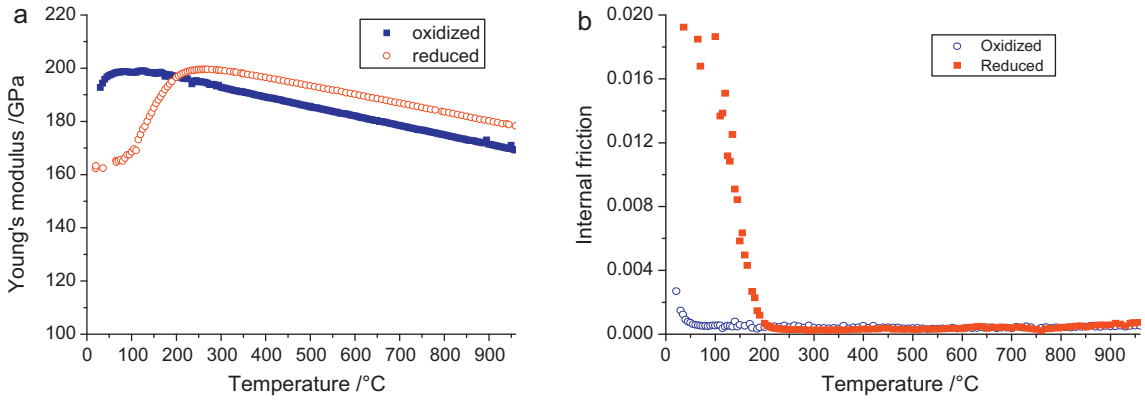

Fig. 4. (a) Young's modulus and (b) internal friction of oxidized and reduced samples measured with the resonance method.

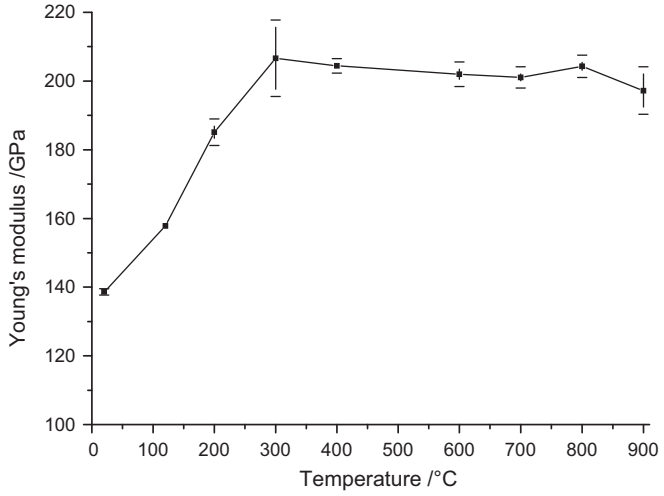

Fig. 5. Young's modulus of the as-received reduced material measured with ring-on-ring test.

used to determine the fracture toughness in air as outlined in [14]. The fracture toughness increases ~34% from RT to 200 °C (Fig. 6). The increase from RT to 200 °C is similar to the effect observed for Young's modulus. The fracture toughness maintains rather stable from 200 °C to 700 °C, and contrary to the Young's modulus it then increases strongly by about 43% from 700 °C to 800 °C.

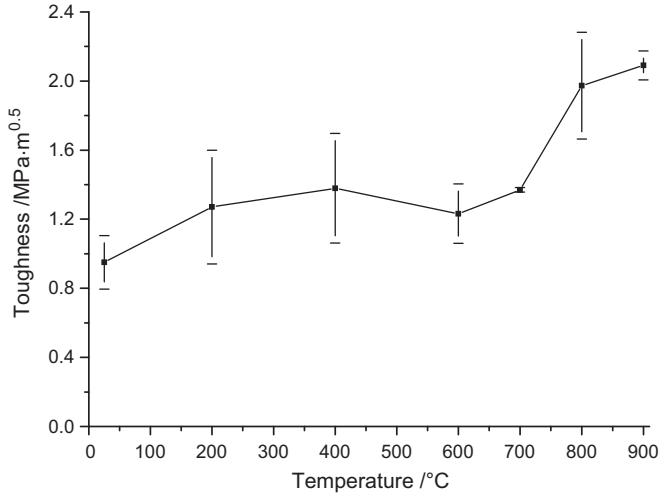

Fig. 6. Fracture toughness measured with ring-on-ring test.

In general, the fracture toughness is defined as $K_{IC} = \sqrt{\gamma \cdot E}$, where γ is fracture energy for brittle materials and E the Young's modulus. For single crystals fractured at defined planes, the fracture energy is proportional to the surface energy [5]. Furthermore the surface energy appears to be proportional to Young's modulus for single crystals [18]. Therefore, K_{IC} of single crystals should be proportional to Young's modulus, which was verified in Ref. [18].

For polycrystalline materials stronger contributions to the fracture energy are due to the crystalline direction of fracture surface, grain size, grain boundary phases, and fracture mode [5]. However, interestingly, also a linear relation between E and K_{IC} has been obtained for polycrystalline materials [19–21]. The fracture toughness and hence also the fracture energy for $Y_{0.07}Sr_{0.895}TiO_3$ at RT and 200 °C are lower compared with other materials with values between that expected for poly- and single crystals (Fig. 7).

It was reported that $SrTiO_3$ transforms from tetragonal to cubic at 105 K [22], and maintains the cubic symmetry above 105 K. To characterize the structure at 350 °C, a specimen was annealed at 350 °C for 24 h in air and then quenched at ambient atmosphere to RT. The sample exhibits a cubic symmetry, which excludes a relationship to a structural change for the increase in Young's modulus and fracture toughness up to around 200 °C.

It has been reported on the basis of compressive tests on single crystals that the cubic $SrTiO_3$ undergoes several brittle-to-ductile transitions [23]. In the work the temperature range has

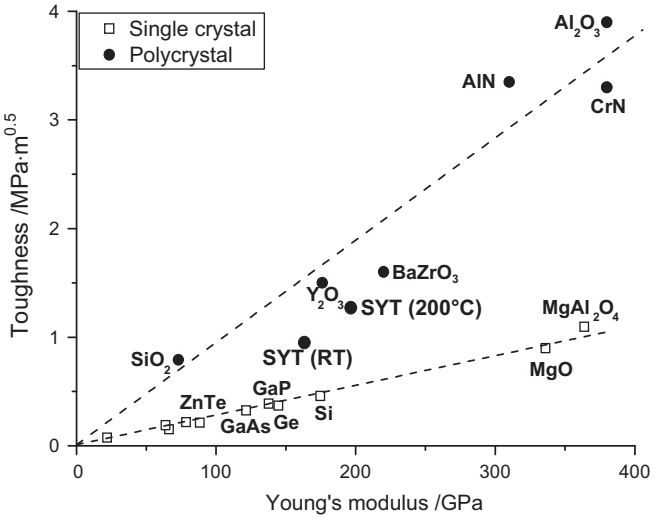

Fig. 7. Relationship of Young's modulus and fracture toughness for ceramics [19–21].

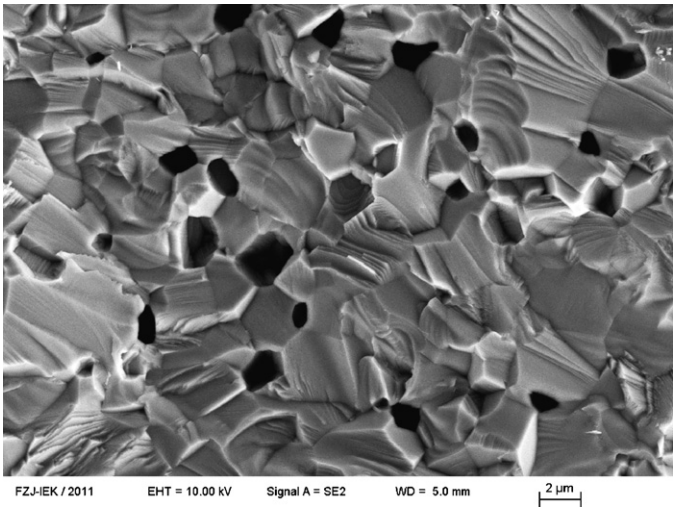

Fig. 8. Micrograph verifying that the samples fracture in a transgranular mode.

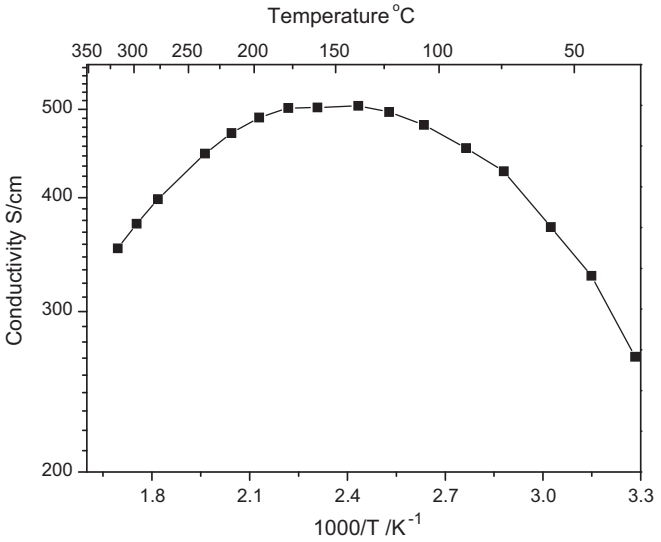

Fig. 9. The conductivity of a reduced sample as a function of the temperature.

been subdivided into four regimes [23,24]: in the ductile regime I (<25 °C), the critical flow stress decreases with increasing temperature; in the ductile regime II (25–700 °C), critical flow stress is almost constant; in the brittle regime III (700–1227 °C), the fracture stress increases with temperature and finally in the ductile regime IV (1227–1538 °C) it decreases with increasing temperature. The low temperature increase in Young's modulus of oxidized $Y_{0.07}Sr_{0.895}TiO_3$ (below 70 °C) might be related to the same origins as the brittle-to-ductile transition. For reduced samples, the transition appears to be shifted to 220 °C. However, the reported brittle-to-ductile transition at 700 °C is neither reflected in Young's modulus nor internal friction reported here.

The increase of fracture toughness from RT to 200 °C might be attributed to the same effect as the increase in Young's modulus. However, whereas the fracture toughness shows a strong increase from 700 °C to 800 °C, the Young's modulus maintains a stable value, suggesting that both properties are not influenced by a single mechanism at higher temperatures.

The fracture toughness of the dense specimens at elevated temperatures was measured in air. No indications of a change from grey for the as received specimens to a white color that is usually an indication of oxidation for this material could be seen. Nevertheless the question if a thin oxide layer might have led to the high fracture toughness values at 800 °C needs to be answered. Although the diffusion rate of oxygen is very low for bulk samples, the crack tips could react with oxygen. To exclude this effect, also the average fracture stress was measured using ring-on-ring bending tests under Ar/2.5% H_2 at RT, 700 °C and 800 °C, respectively. In all tests (RT to 800 °C) the samples fracture in a transgranular mode (Fig. 8).

Contrary to the fracture toughness the average fracture stress increases only slightly from 83 MPa at RT to 121 MPa at 700 °C and remains 122 MPa at 800 °C, which is consistent with Young's modulus. This suggests that the fracture toughness increase from 700 °C to 800 °C could be due to the oxidation of crack tip zone. As discussed above, the lattice expands ~0.2% from reduced to oxidized state. A very thin oxidation layer could induce a compressive stress in the surface and hence at the crack tip zone. Hence, the higher fracture toughness at 800 °C might be due to oxidation in air might be an artifact of the measurement.

3.3. Conductivity

The electrical conductivity of a reduced sample increases from RT to 180 °C, and above it decreases with temperature (Fig. 9). In general, the conductivity is influenced by two thermal effects, first, more charge carriers are thermally activated from valence band to conduction band, which increases the conductivity and second, more scattering of charge carriers by lattice vibration, which decreases the conductivity at higher temperatures. Hence, an effect related to the activation of electrons could be responsible for the increase of the Young's modulus of the reduced material at temperatures below 200 °C (Fig. 4a). Also the higher value of internal friction at low temperatures (Fig. 4b) could be explained by the activation of charge carriers which scattered the vibrations.

3.4. Porosity effect

A substrate porosity of ~30% is required to permit sufficient gas supply to the electrochemically active sites of the functional anode layer. Hence in real application porous substrates are used. Therefore, it is also important to characterize the properties of porous material.

The porosity dependence of the Young's modulus was investigated using indentation testing for tape casted SYT substrates produced at IEK-1 of the Forschungszentrum Jülich (Fig. 10) [25]. It was verified that the Young's modulus is ~190 GPa for a porosity of

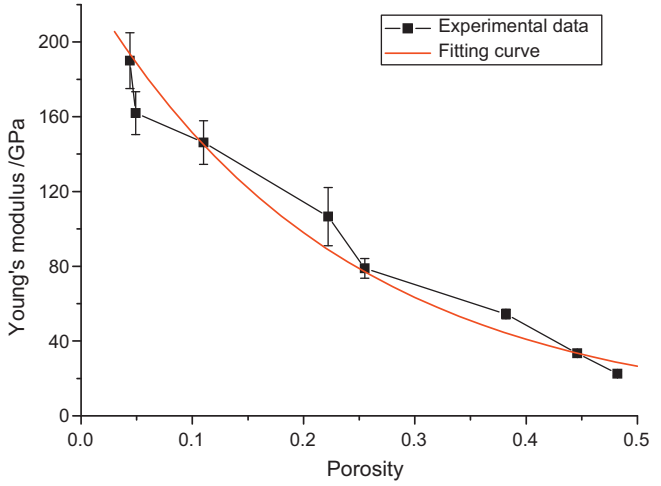

Fig. 10. The porosity dependence of the Young's modulus as described by the equation [26]: $E = E_0 \cdot \exp(-a \cdot P)$.

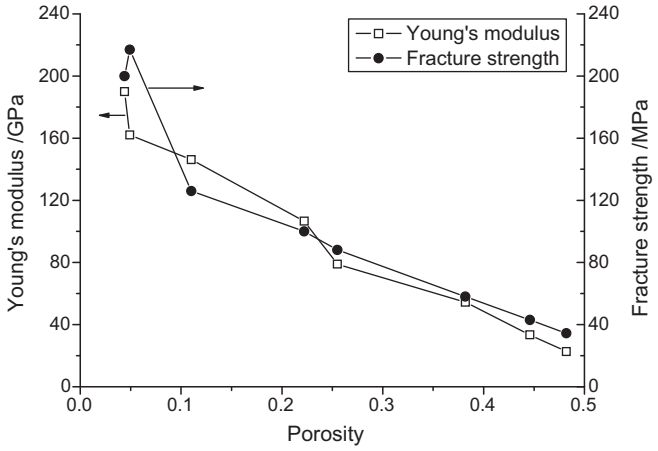

Fig. 11. Comparison of bending strength [25], and Young's modulus.

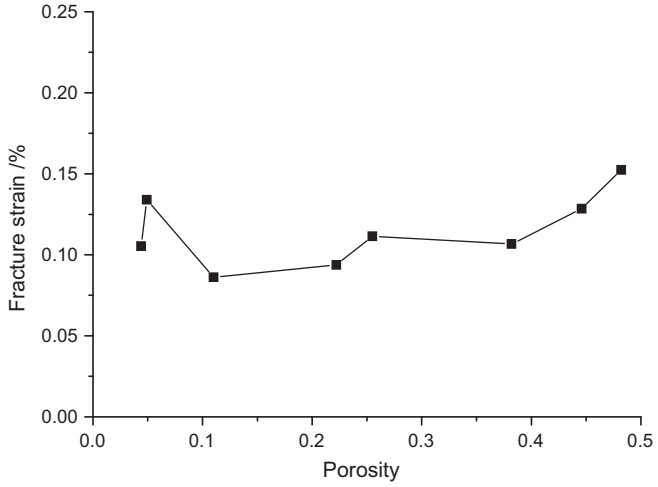

Fig. 12. Critical strain as a function of porosity.

~4% in agreement with the values quoted above and it decreases strongly to ~23 GPa for a porosity of ~48.2%. The porosity dependence of the Young's modulus was described by the equation [26]: $E = E_0 \cdot \exp(-a \cdot P)$, with E_0 Young's modulus at 0 porosity $P = 0$. The experimental data could be well described by a curve with $E_0 = 230$ GPa and $a = 4.4$ (Fig. 10).

The bending strength of the investigated porous SYT materials reported in [25] is compared with the Young's modulus values in Fig. 11. The strength decreases from 214 MPa for a porosity P of ~4% to 34 MPa for a porosity of ~48.2%. The data proof that strength and Young's modulus have almost identical porosity dependencies, which implies that the porosity mainly changes the effective area of the specimens and no additional defects are induced by for example clustering of pores. Interestingly, the fracture strain obtained from strength and Young's modulus increases slightly with increasing porosity after an initial decrease (Fig. 12), which might be an indication of energy consumption by pores in the crack tip deformation zone.

4. Conclusion

The investigated SYT material is very thermo-chemically stable. The change of oxygen stoichiometry δ is only 0.03 from reduced to the oxidized state, whereas on heating from RT to 1000 °C in air the weight change of the oxidized material was insignificant.

The Young's modulus of reduced samples increases by ~20% from RT to 220 °C, and then decreases slightly up to 960 °C. Correspondingly, the internal friction exhibits a peak along with the strong change of Young's modulus. The average fracture stress measured under reduced conditions shows a similar behavior as the Young's modulus. The fracture toughness measured in air increases ~34% from RT to 200 °C, and maintains a stable value from 200 °C to 700 °C, and then increases 43% from 700 °C to 800 °C. The increase of fracture toughness from RT to 200 °C is attributed to the increment of Young's modulus, while the rapid increase from 700 °C to 800 °C might be due to the oxidation at crack tip zone.

Fracture strength and Young's modulus have almost identical porosity dependencies. The fracture strain increases slightly with increasing porosity after an initial decrease, which might be an indication of energy consumption by pores in the crack tip deformation zone.

Acknowledgements

Financial support from the European Commission by the Fuel Cells & Hydrogen Joint Undertaking under the 7th Framework program "SCOTAS" (FCH JU no. 256730) is gratefully acknowledged.

References

[1] T.X. Ho, P. Kosinski, A.C. Hoffmann, A. Vik, International Journal of Hydrogen Energy 34 (2009) 3488–3499.
[2] R.N. Basu, G. Blass, H.P. Buchkremer, D. Stöver, F. Tietz, E. Wessel, I.C. Vinke, Journal of the European Ceramic Society 25 (2005) 463–471.
[3] M. Ettler, H. Timmermann, J. Malzbender, A. Weber, N.H. Menzler, Journal of Power Sources 195 (2010) 5452–5467.
[4] Q.X. Fu, F. Tietz, Fuel Cells 8 (2008) 283–293.
[5] M.W. Barsoum, Fundamentals of Ceramics, 2nd ed., Institute of Physics Publishing (Gb), London, 2003.
[6] J. Malzbender, R.W. Steinbrech, L. Singheiser, Ceramic Engineering and Science Proceedings 26 (2005) 293–297.
[7] N. Christiansen, H. Holm-Larsen, M.J. Jorgensen, P.V. Hendriksen, A. Hagen, S. Ramousse, M. Wandel, ECS Meeting Abstracts 902 (2009) 1217.
[8] D. Simwonis, H. Thülen, F.J. Dias, A. Naoumidis, D. Stöver, Journal of Materials Processing Technology 92–93 (1999) 107–111.
[9] J. Malzbender, J.M.J. den Toonder, A.R. Balkenende, G. de With, Materials Science and Engineering: R: Reports 36 (2002) 47–103.
[10] W.C. Oliver, G.M. Pharr, Journal of Materials Research 7 (1992) 1564–1583.
[11] J. Malzbender, G. de With, Surface and Coatings Technology 137 (2001) 72–76.
[12] P. Chantikul, G.R. Anstis, B.R. Lawn, D.B. Marshall, Journal of the American Ceramic Society 64 (1981) 539–543.
[13] G.R. Anstis, P. Chantikul, B.R. Lawn, D.B. Marshall, Journal of the American Ceramic Society 64 (1981) 533–538.
[14] B.X. Huang, A. Chanda, R.W. Steinbrech, J. Malzbender, Journal of Materials Science 47 (2012) 2695–2699.
[15] H. Fessler, D.C. Fricker, Journal of the American Ceramic Society 67 (1984) 582–588.
[16] T. Fett, G. Rizzi, J.P. Guin, S.M. Wiederhorn, Journal of Materials Science 42 (2007) 393–395.
[17] J.B. Watchman, Mechanical Properties of Ceramics, Wiley & Sons, New York, 1996.
[18] S. Freiman, J. Mecholsky, Journal of Materials Science 45 (2010) 4063–4066.
[19] I.C. Albayrak, S. Basu, A. Sakulich, O. Yeheskel, M.W. Barsoum, Journal of the American Ceramic Society 93 (2010) 2028–2034.
[20] M. Asmani, C. Kermel, A. Leriche, M. Ourak, Journal of the European Ceramic Society 21 (2001) 1081–1086.
[21] W. Feng, D. Yan, J. He, G. Zhang, G. Chen, W. Gu, S. Yang, Applied Surface Science 243 (2005) 204–213.
[22] E.K.H. Salje, et al., Journal of Physics: Condensed Matter 10 (1998) 5535.
[23] P. Gumbsch, S. Taeri-Baghbadrani, D. Brunner, W. Sigle, M. Rühle, Physical Review Letters 87 (2001) 085505.
[24] D. Brunner, S. Taeri-Baghbadrani, W. Sigle, M. Rühle, Journal of the American Ceramic Society 84 (2001) 1161–1163.
[25] P. Vozdecky, A. Roosen, Q. Ma, F. Tietz, H. Buchkremer, Journal of Materials Science 46 (2011) 3493–3499.
[26] A.R. Boccaccini, Z. Fan, Ceramics International 23 (1997) 239–245.